

# Deep learning-based photoacoustic imaging of vascular network through thick porous media

Ya Gao<sup>1,2</sup>, Wenyi Xu<sup>1</sup>, Yiming Chen<sup>1,2</sup>, Weiya Xie<sup>1,2</sup>, Qian Cheng<sup>1,2,3\*</sup>

<sup>1</sup>Institute of Acoustics, School of Physics Science and Engineering, Tongji University, Shanghai, PR China

<sup>2</sup>The Key Laboratory of Spine and Spinal Cord Injury Repair and Regeneration, Ministry of Education, Tongji University, Shanghai, PR China.

<sup>3</sup>Shanghai Research Institute for Intelligent Autonomous Systems, Shanghai, PR China.

\*Corresponding authors: [q.cheng@tongji.edu.cn](mailto:q.cheng@tongji.edu.cn)

## Abstract

Photoacoustic imaging (PAI) is a promising approach to realize *in vivo* transcranial cerebral vascular imaging. However, the strong attenuation and distortion of the photoacoustic wave caused by the thick porous skull greatly affect the imaging quality. In this study, we designed a convolutional neural network (CNN) with a U-Net architecture to extract the effective photoacoustic information hidden in the speckle patterns; obtained vascular network images datasets under porous media through simulation and experiment, and trained the network weights respectively. The results show that the proposed neural network can learn the mapping relationship between the speckle pattern and the target; extract the photoacoustic signals of some vessels submerged in noise to reconstruct high-quality images with a sharp outline of the vessel and clean background. Compared with the traditional photoacoustic reconstruction method, the deep learning-based reconstruction algorithms can achieve better performance, the mean absolute error (MAE), Structural SIMilarity (SSIM) and peak signal-to-noise ratio (PSNR) of reconstructed images have been greatly improved. In conclusion, the proposed neural network can effectively extract valid information from highly blurred speckle patterns for the rapid reconstruction of target images, which offers promising applications in transcranial photoacoustic imaging.

## I. Introduction

Human brain mapping is one of most exciting research areas in contemporary medical imaging. Currently, brain imaging is performed by magnetic resonance imaging (MRI), computer tomography (CT), and near-infrared spectroscopy (NIRS); however, because of the inherent limitations of the above imaging mechanisms (such as imaging speed, safety, imaging resolution, etc.), it is impossible to characterize the physiological activity of the brain entirely. Photoacoustic imaging (PAI) is a promising medical imaging modality that uses a short electromagnetic pulse to generate ultrasound waves based on the thermoelastic effect. The imaging mechanism based on the photoacoustic effect allows us to obtain a high contrast in optical imaging and a high spatial resolution in ultrasound imaging. The high contrast is attributed to the high sensitivity of light to the absorption of biomolecules such as hemoglobin during the photoacoustic excitation phase. Further, the high spatial resolution is attributed to the detection of ultrasonic waves during the photoacoustic emission phase. Wang et al. were the first to apply photoacoustic tomography to the brain imaging of mice and successfully obtain the structural images of mouse brain with a penetration depth of 8 mm and a resolution of 0.2 mm [1]. Jiang et al. developed a wearable multispectral three-dimensional photoacoustic brain imaging system for rats with

a resolution of 0.2 mm [2]. Razansky et al. [3], Luo et al. [4], and Nie et al. [5] reported outstanding work in the field of photoacoustic brain imaging. This study focuses on mice and rats with thin skulls (around 0.3–0.8 mm); we do not focus on the human skull because it is a thick porous media that causes strong scattering of photoacoustic signals.

Imaging through thick porous media has long plagued the field of medical imaging. Because of the strong scattering of the skull, both light and ultrasound imaging suffer from the interference of multiple scattering times, and this leads to the distorted propagation direction and wavefront information. Thus, it is difficult to achieve high-resolution images to observe changes in tissue morphology and structure caused by intracranial disease or injury.

In recent years, the development of computational optical imaging has further promoted the related research of scattering imaging. Current scattering imaging methods mainly include wavefront shaping and speckle-related imaging. Wavefront shaping aims to obtain a scattering matrix [6] that describes the light transmission trajectory inside the medium. The incident field is reversely designed to achieve focusing and imaging at any position. A variety of wavefront shaping methods have been developed, which includes feedback-based wavefront shaping [7], transmission matrix measurements [8, 9], and optical phase conjugation [10-12]. Besides, it is easy to produce a speckle pattern with a granular intensity distribution when the surface of an object is irradiated by a highly coherent laser. Feng and Freund et al. proposed that the light field after light passes through a strong scattering medium retains information carried by the incident beam (i.e., optical memory effect) [13,14]. Further, based on feedback wavefront shaping technology, Wang et al. proposed non-linear photo-acoustically guided wavefront shaping (PAWS), where photoacoustic signals were used as “guide stars” to obtain feedback signals and guide iterative wavefront optimization to achieve focusing within and after the scattering medium [15].

Artificial intelligence, especially deep learning technology, is rapidly developing and widely used in computational imaging; it solves some long-standing problems in the fields of scattering imaging [16-18], sparse data or limited-view imaging [19-21], phase recovery [22-24], super-resolution imaging [25-27], and other fields. Ando et al. first proposed the use of support vector regression (SVR) to perform binary classification of the speckle intensity maps corresponding to the collected face and non-face data by mapping them to a high-dimensional feature space [16]. Unlike traditional machine learning algorithms, the deep learning multilayer network structure has a strong fitting ability that can fit the mapping relationship of the imaging system containing scattering media. Lyu et al. built a hybrid neural network to achieve the recovery of handwritten digits and letters through a strong scattering medium [17]. Li et al. used trained neural networks to predict untrained scattering media and different types of imaging targets; it could reconstruct object images [18]. Therefore, it shows that neural networks can autonomously mine and utilize the hidden physical statistical invariance based on high-quality data.

Based on PAI applied to the biggest challenge of sound scattering in brain imaging, a deep learning method is used to build a CNN network structure to extract “hidden” effective information. High-quality photoacoustic images of vascular networks through thick scattering media were obtained in experiments and simulations, respectively.

The overview of the paper is organized as follows. In Section II, we analyzed the generation and propagation of transcranial photoacoustic signals, including the physical model of PA imaging reconstruction and how to use CNN to optimize low-quality images. This section also introduces the proposed network architecture, simulation and experimental data acquisition in detail. Section III provides details for reconstruction results of simulations and experiments, as well as evaluation indicators. Then, some discussion about the results and the limitations of this method is introduced in Section IV. Finally, we summarized the research and provided prospects for future work.

## II. Materials and Methods

### A. Photoacoustic Propagation Process

As an example, for intracranial vascular imaging, PAI can be performed as follows: 1) On the outer side of the skull, the pulsed laser emits laser light with a characteristic absorption wavelength of hemoglobin; the light energy passes through the skull; 2) The characteristic absorption of hemoglobin in cerebral blood vessels in the brain is simulated; 3) Ultrasound wave is generated based on the photoacoustic effect; 4) Ultrasound carrying blood vessel information propagates outside the skull and is strongly scattered by the skull; 5) Array transducer outside the skull is used to receive the scattered ultrasound and reconstruct the intracranial blood vessel distribution.

As light offers energy and ultrasound offers wave information for PAI, the effect of ultrasonic scattering on PA image quality is considerably more serious than light scattering. The conversion of the photoacoustic effect [28] follows

$$\left( \nabla^2 - \frac{1}{v_s^2} \frac{\partial^2}{\partial t^2} \right) p(\vec{r}, t) = -\frac{\beta}{C_p} \frac{\partial H}{\partial t}$$

where  $v_s$  denotes the speed of sound,  $p(\vec{r}, t)$  represents the sound pressure at position  $\vec{r}$  and time  $t$ ,  $\beta$  represents the thermal expansion coefficient of volume expansion, and  $C_p$  represents isobaric specific heat capacity. Further,  $H$  denotes the heat source function, which is defined as the conversion of light energy to heat energy per unit volume and unit time.

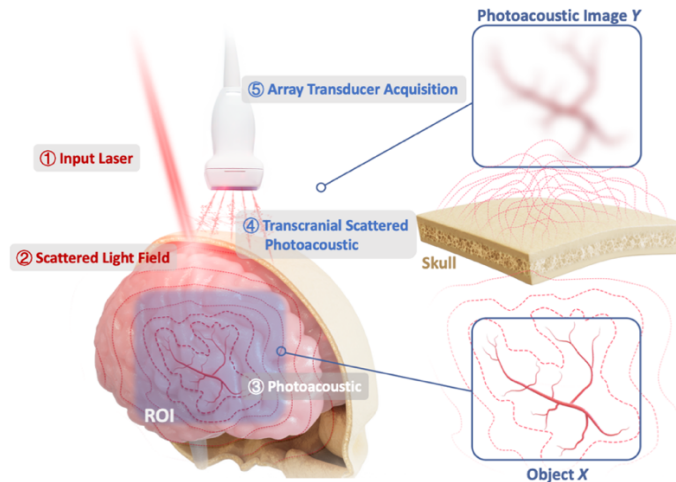


**Fig. 1.** Schematic of the physical transmission process of photoacoustic brain imaging.

In the above process, ultrasonic scattering has a considerably more serious effect on image quality than light scattering because the light offers energy whereas the ultrasound offers wave information for PAI. Blood vessel distribution can be considered the measuring object  $X$ , the extracranial photoacoustic signal can be considered the measured distribution  $Y$ , and the process from  $X$  to  $Y$ , the forward propagation process of the photoacoustic signal through the skull. This process can be regarded as a mapping function  $F$ , and the whole process can be described by a mapping  $F: X$  to  $Y$ . The problem can then be transformed into solving an optimization problem for obtaining object information  $X$ . Now, deep learning[29] methods can be used to solve the problem.

$$\hat{X} = \operatorname{argmin}[\|F(X) - Y\|_2^2 + \alpha\Phi(X)]$$

## B. Network Architecture

We build a CNN to learn a statistical model relating the speckle patterns and unscattered objects. The overall structure of the proposed CNN (Fig. 2) follows a modified encoder–decoder “U-Net” architecture [30]. In view of the difference in the distribution thickness and strength of the blood vessel network image, batch normalization is performed after the pooling layer, and therefore, the data distribution is relatively stable; the next step of convolution is performed. The input of CNN is a pre-processed  $128 \times 128$  pixels speckle pattern, and then, through the “encoder” path, the intermediate output from the encoder has small lateral dimensions but rich depth information. Next, the low-resolution image goes through the “decoder” path, and the information of different spatial scales is transmitted and fused through a skip connection to retain high-frequency information. Finally, a convolutional layer is used to output a specified size image based on the required imaging task.

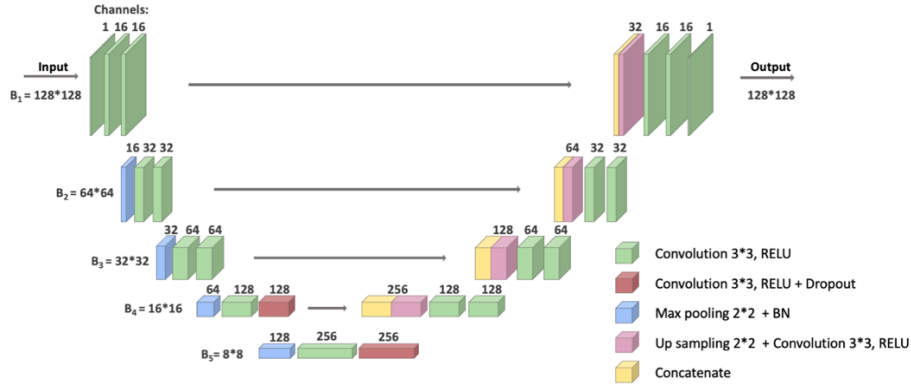


**Fig. 2.** Proposed CNN model. The number written above each layer indicates the number of convolution kernels (channels). The numbers B1, ..., B5 represents the size of the image (the block size in the weight matrix), which remains unchanged in each row.

## C. Simulation Datasets

In the simulation, we used hand-segmented blood vessel images (Fig. 3A) in the public DRIVE (Digital Retinal Images for Vessel Extraction) dataset, which is a total of 40 images. Then, each image was segmented by a sliding window so that each image has blood vessels of different lengths, widths, tortuosity, branching patterns, and angles. Finally, a total of 4000 blood vessel images were obtained

(Fig. 3B). The open-source k-Wave MATLAB Toolbox was used to simulate the propagation of photoacoustic waves of blood vessels in porous media. The simulation settings are shown in Fig. 3C. First, the segmented blood vessel image was binarized and placed in a grid as a photoacoustic source with a porous medium simulating the skull above it. Then, the photoacoustic signal passing through the porous medium was received by an ultrasound array probe. The propagation process from 0  $\mu\text{s}$  to 18  $\mu\text{s}$  is shown in Fig. 3D. Finally, the detected photoacoustic signal was reconstructed by delay and sum (DAS). In addition, according to the parameters of the skull, the thickness, sound velocity, and density of the porous medium were set to 2.1 mm, 4100 m/s, and 1500 kg/m<sup>3</sup> [31,32]; the rest are set to soft tissues with the sound velocity and density of 1500 m/s and 1000 kg/m<sup>3</sup>, respectively.

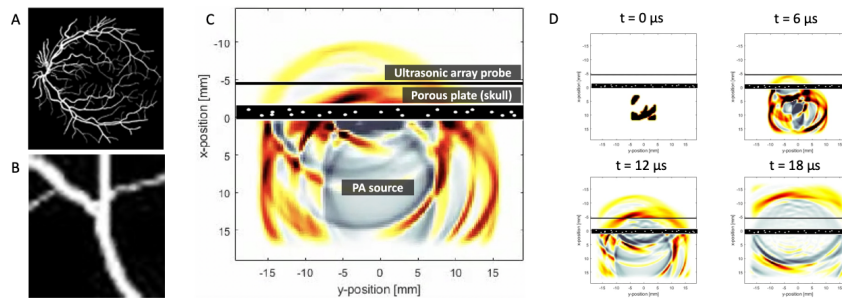


**Fig. 3.** Simulation of PA signal propagation. (A) Fundus blood vessel image. (B) Segmented blood vessel image from (A) used as the photoacoustic source of (C). (C) Simulation setup in k-Wave. (D) Propagation process of photoacoustic waves from t = 0 to t = 18  $\mu\text{s}$ .

#### D. Experiment Datasets

Coral branches (about 0.8–1.5 mm in diameter) were used to simulate the blood vessel network, and they are buried in the phantom. A phantom layer embedded with transparent crystal particles (about 100–500  $\mu\text{m}$  in diameter, which corresponds to an ultrasonic frequency of 3–15 MHz) is placed above it to simulate a porous medium, and an ultrasonic array probe (center frequency: 10 MHz) is used on its outside to receive scattered photoacoustic signals from the blood vessels. Then, the porous medium is replaced with a phantom layer with the same thickness as the scattering layer to receive the unscattered photoacoustic signal from the blood vessels. The instrument for collecting signals and imaging is a self-developed PAI system. A total of 1000 pairs of images of the blood vessel network with and without scattering were collected.

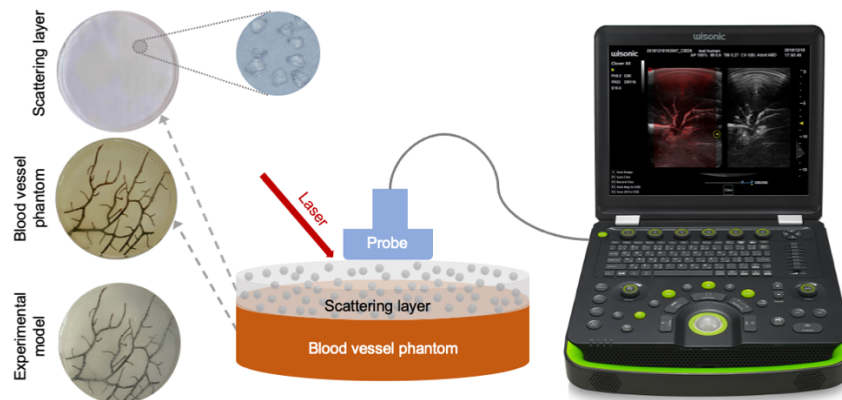


**Fig. 4.** Experimental setup. On the left are the scattering layer used in the experiment (including the micrograph of the transparent crystal particles), blood vessel phantom, and combined experimental phantom. The positions of the laser and the probe are shown in the middle using a home-made PAI system (on the right) for acquisition.

### E. Evaluation and implementation

In this study, we choose mean absolute error (MAE) as the loss function and Adam as the strategy to update the weights during the training process. MAE, which measures the deviation of each pixel of the image from the average pixel; Structural SIMilarity (SSIM), which measures the similarity of each pair of image brightness, contrast, and structure; and peak signal-to-noise ratio (PSNR), which objectively indicates image quality, are the three performance indicators selected for evaluation. The neural network was implemented in Keras with the Tensorflow backend (<https://keras.io>). All calculations were conducted on a computer with CPU Intel Xeon Gold 6130 CPU @ 2.10 GHz, GPU NVIDIA Quadro P4000, and 1024G of RAM.

## III. Results

### A. Simulation Results

We obtained nine pairs of speckle images corresponding to other segmentation patterns from the DRIVE database but not in the training set; we sent them to the trained neural network to test the performance of the network on simulated data. The ground truth images in the segmentation database are shown in Fig. 5A; speckle images obtained by simulation are shown in Fig. 5B; and reconstructed images output by CNN are shown in Fig. 5C. Compared with ground truth images, speckle images cause strong acoustic scattering and acoustic impedance mismatch of photoacoustic waves because of the porous structure of the skull and the difference in acoustic impedance with blood vessel tissues. This can lead to serious speckle artifacts, loss of detail information, and blurred edges; further, it seriously degrades the image quality. The CNN output image effectively reconstructs the important features of the target, and it shows a clear edge and a clean background.

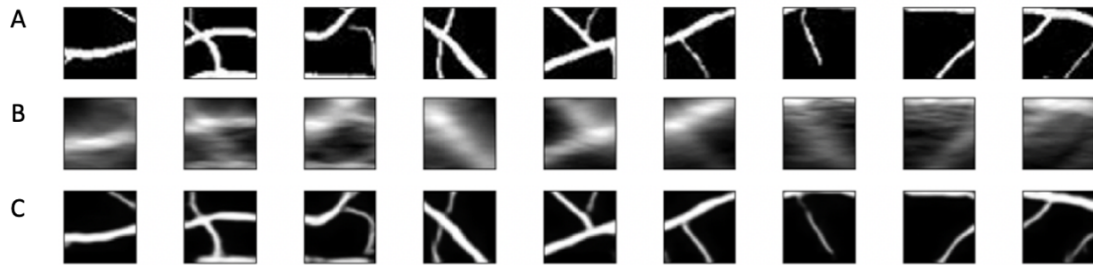


**Fig. 5.** Reconstructed results of the simulation. (A) Ground truth images in the segmentation database. (B) DAS reconstruction. (C) Reconstruction using the proposed CNN.

### B. Experiment Results

Similar to the simulation, nine pairs of images are obtained from the experimental data; the images (Fig. 6B) collected by the scattering layer are input into the trained neural network. Then, the output reconstructed image (Fig. 6C) is compared with the image collected by the non-scattering layer (Fig.

6A). The images collected by the scattering layer are accompanied by strong speckle and background noise. A clearer blood vessel shape can be obtained after training.

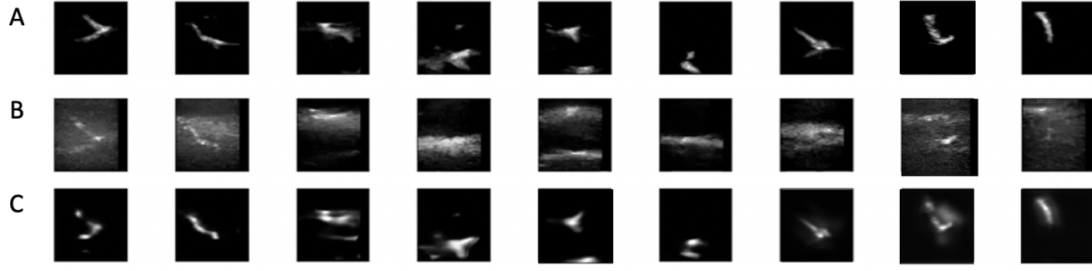


**Fig. 6.** Reconstructed results of the Experiment. (A) Images without scattering layer. (B) Images with scattering layer. (C) Reconstruction using the proposed CNN.

### C. Performance Evaluation

Tab. 1 lists the MAE, SSIM, and PSNR of all test samples reconstructed by DAS and CNN from the test sets (100 pairs in total) of the simulation and the experiment, respectively. The method based on CNN has an obviously better performance than DAS, and the three evaluation indexes of MAE, SSIM and PSNR are greatly improved in the simulation and the experiment. Further, it can quantitatively explain that the blood vessel image reconstructed by CNN from the speckle image is very helpful in terms of accuracy, brightness, contrast, structural similarity, and image quality.

Metrics	Simulation		Experiment	
	DAS	CNN	DAS	CNN
MAE	0.450	0.065	0.042	0.007
SSIM	0.050	0.610	0.427	0.933
PSNR	6.184	16.622	21.583	28.450

**Tab. 1.** Performance Comparison of the DAS and CNN.

## IV. Discussion

We investigated a method for the PAI of blood vessel networks through thick porous media based on deep learning post-processing. The advantages and benefits of PAI are based on the condition that biological tissues have relatively uniform acoustic characteristics. Hard and porous skull and soft brain tissues cause strong acoustic impedance mismatch and scattering, and then, time-domain reconstruction algorithms lead to serious speckle noise and scattering artifacts. Inspired by the performance improvement of CNN in medical imaging, we adopted a combination of CNN and DAS reconstruction algorithms. We captured photoacoustic images without/with the scattering layer as the learning target and the network input, respectively. Using the feature mining of CNN to decode the complex code of the porous structure, the results show that this method successfully removes speckles and artifacts and outputs a photoacoustic image close to the real blood vessel network. It is worth mentioning that we use B-mode for imaging. Compared with C-mode, which is commonly used in brain imaging, it not only needs to overcome the scattering through the skull, but also needs to provide more information in the depth direction.

The thickness and structure distribution of skulls are considerably different for various body types animals, and therefore, the photoacoustic images are disturbed to varying degrees. However, a CT or MRI scan on each skull used to analyze the characteristics of the porous media and assess the degree of disturbance is a computationally extensive and complex task. Therefore, the evaluation and comparison of the scattering degree caused by porous media based on only photoacoustic images and the ground truth has gained considerable research interest.

Further, the analysis of the spatial frequency of the photoacoustic images is expected to provide a solution for the quantitative evaluation of the image scattering degree caused by porous media. The fewer high-frequency components of the image spatial spectrum, the less detailed is the information of the image, and the more blurred is the image. Therefore, the greater the scattering degree, the greater is the degradation of image quality [33]. The scattering degree can be quantitatively evaluated by the slope of the spatial spectrum. Similarly, this parameter also has the potential to be used as an evaluation index to measure the image reconstruction quality of the neural network.

In this study, we consider the test data set (100 sets of images in total) in the simulation data as an example, and we calculate the slopes of the spatial spectra of the real image, speckle image, and training image (Fig. 7). Owing to the scattering effect of porous media, the spatial spectrum distribution of the ground truth and speckle images is considerably different; however, the spatial spectrum distribution of the image obtained by training has good consistency with the ground truth, which shows that the spatial spectrum of the image can be reconstructed well through training. The spatial frequency spectrum has the potential to be used in cranial image reconstruction. The skull can be regarded as a stable spatial frequency spectrum transmission system. Under appropriate conditions, the transfer function can be obtained using the full spatial spectrum for excitation, and therefore, vascular network imaging that is not affected by the skull can be obtained by deconvolution.

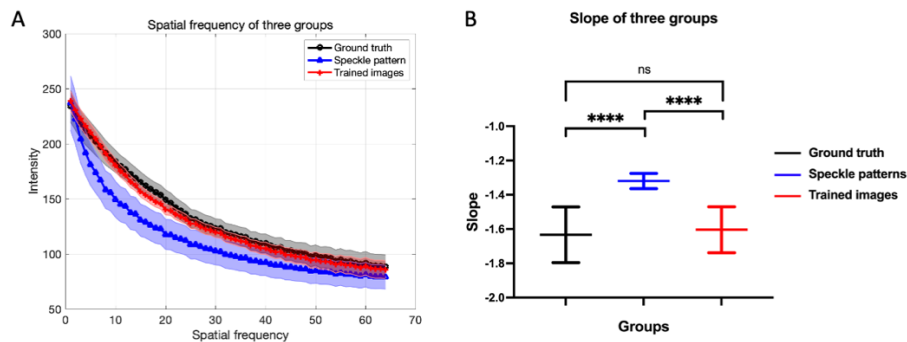


**Fig. 7.** Comparison of spatial frequency of three groups through simulation. (A) Spatial frequency distribution of three groups of images. (B) The slope of the spatial spectrum of the three sets of images.

In this method, the photoacoustic image of the blood vessel with or without disturbance is acquired based on a specific porous structure, then CNN learning is performed based on the data-driven approach, and the final output photoacoustic image is close to the real blood vessel network. Therefore, the CNN can only be used for photoacoustic image reconstruction of the specific porous structure. Each skull has a different but similar structural distribution. Based on the successful prediction of multiple learned scatter plates versus unlearned scatter plates[18], there is a possibility for the clinical

citation of this method. Through the learning of multiple isolated skulls, CNN can finally learn the general porous characteristics of the skull to reconstruct high-quality photoacoustic images.

However, this method has some limitations, such as the high cost and time-consuming data acquisition and network training in the early stage. A trained network is difficult to apply to other imaging systems; its universality and flexibility are not sufficient. Most importantly, although the current deep learning method can provide the mapping relationship between the input and output of an imaging system, it cannot reveal the physical mechanism of sound propagation in porous media. Many researchers have noticed this problem and attempted to integrate physical relationship with deep learning [34]. Physical relationship is used to constrain and correct learning objectives, and deep learning is used to make physical relationship more experimental. Many achievements have shown that deep learning will help make more breakthroughs and progress in the imaging field.

The method is currently based on a specific porous structure to obtain photoacoustic images of blood vessels with or without disturbances, and learn in the form of data-driven. Finally, the photoacoustic image close to the real vascular network is output, so the CNN can only be used for photoacoustic image reconstruction of this porous structure. Due to the specificity of the organism, each skull has a different but similar structural distribution. Based on the successful prediction of multiple learned scatter plates versus unlearned scatter plates[18], it provides the possibility for the clinical citation of this method. Through the learning of multiple isolated skulls, CNN can finally learn the general porous characteristics of the skull to reconstruct high-quality photoacoustic images.

## **V. Conclusion**

We have demonstrated a CNN with a U-Net structure to effectively extract effective information from highly blurred speckle patterns to reconstruct the target image quickly. In addition, the relationship between the spatial frequency of the photoacoustic image and the degree of scattering was studied.

As inherent in all learning approaches, the limitation of the proposed method is dictated by the quality of the training data. In future research, we will consider combing the CNN with a physical model, and a series of PAI experiments of intracranial blood vessels in rabbits and humans will be studied to further verify the effectiveness of deep learning methods in scattering decoding.

## Reference:

- [1] X. Wang, Y. Pang, G. Ku, X. Xie, G. Stoica, and L. V. Wang, "Noninvasive laser-induced photoacoustic tomography for structural and functional in vivo imaging of the brain," *Nat. Biotechnol.*, vol. 21, no. 7, Art. no. 7, Jul. 2003, doi: 10.1038/nbt839.
- [2] J. Tang, J. E. Coleman, X. Dai, and H. Jiang, "Wearable 3-D Photoacoustic Tomography for Functional Brain Imaging in Behaving Rats," *Sci. Rep.*, vol. 6, no. 1, Art. no. 1, May 2016, doi: 10.1038/srep25470.
- [3] P. Subochev *et al.*, "Toward whole-brain in vivo optoacoustic angiography of rodents: modeling and experimental observations," *Biomed. Opt. Express*, vol. 11, no. 3, pp. 1477–1488, Mar. 2020, doi: 10.1364/BOE.377670.
- [4] X. Yang *et al.*, "Skull Optical Clearing Solution for Enhancing Ultrasonic and Photoacoustic Imaging," *IEEE Trans. Med. Imaging*, vol. 35, no. 8, pp. 1903–1906, Aug. 2016, doi: 10.1109/TMI.2016.2528284.
- [5] W. Li *et al.*, "In Vivo Photoacoustic Imaging of Brain Injury and Rehabilitation by High-Efficient Near-Infrared Dye Labeled Mesenchymal Stem Cells with Enhanced Brain Barrier Permeability," *Adv. Sci.*, vol. 5, no. 2, p. 1700277, 2018, doi: <https://doi.org/10.1002/advs.201700277>.
- [6] C. W. J. Beenakker, "Random-matrix theory of quantum transport," *Rev. Mod. Phys.*, vol. 69, no. 3, pp. 731–808, Jul. 1997, doi: 10.1103/RevModPhys.69.731.
- [7] I. M. Vellekoop and A. P. Mosk, "Focusing coherent light through opaque strongly scattering media," *Opt. Lett.*, vol. 32, no. 16, pp. 2309–2311, Aug. 2007, doi: 10.1364/OL.32.002309.
- [8] S. M. Popoff, G. Lerosey, R. Carminati, M. Fink, A. C. Boccara, and S. Gigan, "Measuring the Transmission Matrix in Optics: An Approach to the Study and Control of Light Propagation in Disordered Media," *Phys. Rev. Lett.*, vol. 104, no. 10, p. 100601, Mar. 2010, doi: 10.1103/PhysRevLett.104.100601.
- [9] M. Cui, "A high speed wavefront determination method based on spatial frequency modulations for focusing light through random scattering media," *Opt. Express*, vol. 19, no. 4, pp. 2989–2995, Feb. 2011, doi: 10.1364/OE.19.002989.
- [10] Z. Yaqoob, D. Psaltis, M. S. Feld, and C. Yang, "Optical phase conjugation for turbidity suppression in biological samples," *Nat. Photonics*, vol. 2, no. 2, Art. no. 2, Feb. 2008, doi: 10.1038/nphoton.2007.297.
- [11] M. Cui and C. Yang, "Implementation of a digital optical phase conjugation system and its application to study the robustness of turbidity suppression by phase conjugation," *Opt. Express*, vol. 18, no. 4, pp. 3444–3455, Feb. 2010, doi: 10.1364/OE.18.003444.
- [12] C.-L. Hsieh, Y. Pu, R. Grange, and D. Psaltis, "Digital phase conjugation of second harmonic radiation emitted by nanoparticles in turbid media," *Opt. Express*, vol. 18, no. 12, pp. 12283–12290, Jun. 2010, doi: 10.1364/OE.18.012283.
- [13] S. Feng, C. Kane, P. A. Lee, and A. D. Stone, "Correlations and Fluctuations of Coherent Wave Transmission through Disordered Media," *Phys. Rev. Lett.*, vol. 61, no. 7, pp. 834–837, Aug. 1988, doi: 10.1103/PhysRevLett.61.834.
- [14] I. Freund, M. Rosenbluh, and S. Feng, "Memory Effects in Propagation of Optical Waves through Disordered Media," *Phys. Rev. Lett.*, vol. 61, no. 20, pp. 2328–2331, Nov. 1988, doi: 10.1103/PhysRevLett.61.2328.

- [15] P. Lai, L. Wang, J. W. Tay, and L. V. Wang, "Photoacoustically guided wavefront shaping for enhanced optical focusing in scattering media," *Nat. Photonics*, vol. 9, no. 2, Art. no. 2, Feb. 2015, doi: 10.1038/nphoton.2014.322.
- [16] T. Ando, R. Horisaki, and J. Tanida, "Speckle-learning-based object recognition through scattering media," *Opt. Express*, vol. 23, no. 26, pp. 33902–33910, Dec. 2015, doi: 10.1364/OE.23.033902.
- [17] M. Lyu, H. Wang, G. Li, S. Zheng, and G. Situ, "Learning-based lensless imaging through optically thick scattering media," *Adv. Photonics*, vol. 1, no. 3, p. 036002, Jun. 2019, doi: 10.1117/1.AP.1.3.036002.
- [18] Y. Li, Y. Xue, and L. Tian, "Deep speckle correlation: a deep learning approach toward scalable imaging through scattering media," *Optica*, vol. 5, no. 10, pp. 1181–1190, Oct. 2018, doi: 10.1364/OPTICA.5.001181.
- [19] "Deep learning optoacoustic tomography with sparse data | Nature Machine Intelligence." <https://www.nature.com/articles/s42256-019-0095-3#Sec1> (accessed Mar. 22, 2021).
- [20] A. Hauptmann *et al.*, "Model-Based Learning for Accelerated, Limited-View 3-D Photoacoustic Tomography," *IEEE Trans. Med. Imaging*, vol. 37, no. 6, pp. 1382–1393, Jun. 2018, doi: 10.1109/TMI.2018.2820382.
- [21] K. H. Jin, M. T. McCann, E. Froustey, and M. Unser, "Deep Convolutional Neural Network for Inverse Problems in Imaging," *IEEE Trans. Image Process.*, vol. 26, no. 9, pp. 4509–4522, Sep. 2017, doi: 10.1109/TIP.2017.2713099.
- [22] A. Sinha, J. Lee, S. Li, and G. Barbastathis, "Lensless computational imaging through deep learning," *Optica*, vol. 4, no. 9, pp. 1117–1125, Sep. 2017, doi: 10.1364/OPTICA.4.001117.
- [23] Y. Rivenson, T. Liu, Z. Wei, Y. Zhang, K. de Haan, and A. Ozcan, "PhaseStain: the digital staining of label-free quantitative phase microscopy images using deep learning," *Light Sci. Appl.*, vol. 8, no. 1, Art. no. 1, Feb. 2019, doi: 10.1038/s41377-019-0129-y.
- [24] Y. Xue, S. Cheng, Y. Li, and L. Tian, "Reliable deep-learning-based phase imaging with uncertainty quantification," *Optica*, vol. 6, no. 5, pp. 618–629, May 2019, doi: 10.1364/OPTICA.6.000618.
- [25] T. Liu *et al.*, "Deep learning-based super-resolution in coherent imaging systems," *Sci. Rep.*, vol. 9, no. 1, Art. no. 1, Mar. 2019, doi: 10.1038/s41598-019-40554-1.
- [26] E. Nehme, L. E. Weiss, T. Michaeli, and Y. Shechtman, "Deep-STORM: super-resolution single-molecule microscopy by deep learning," *Optica*, vol. 5, no. 4, pp. 458–464, Apr. 2018, doi: 10.1364/OPTICA.5.000458.
- [27] H. Wang *et al.*, "Deep learning enables cross-modality super-resolution in fluorescence microscopy," *Nat. Methods*, vol. 16, no. 1, Art. no. 1, Jan. 2019, doi: 10.1038/s41592-018-0239-0.
- [28] M. Xu and L. V. Wang, "Photoacoustic imaging in biomedicine," *Rev. Sci. Instrum.*, vol. 77, no. 4, p. 041101, Apr. 2006, doi: 10.1063/1.2195024.
- [29] K. G. Kim, "Book Review: Deep Learning," *Healthc. Inform. Res.*, vol. 22, no. 4, p. 351, 2016, doi: 10.4258/hir.2016.22.4.351.
- [30] O. Ronneberger, P. Fischer, and T. Brox, "U-Net: Convolutional Networks for Biomedical Image Segmentation," in *Medical Image Computing and Computer-Assisted Intervention – MICCAI 2015*, Cham, 2015, pp. 234–241, doi: 10.1007/978-3-319-24574-4\_28.
- [31] "Evaluation of Skull Cortical Thickness Changes With Age and Sex From Computed Tomography Scans - Lillie - 2016 - Journal of Bone and Mineral Research - Wiley Online

Library.” <https://asbmr.onlinelibrary.wiley.com/doi/full/10.1002/jbmr.2613> (accessed Mar. 22, 2021).

[32] “Appendix A: Typical Acoustic Properties of Tissues,” in *Basics of Biomedical Ultrasound for Engineers*, John Wiley & Sons, Ltd, 2010, pp. 313–314.

[33] “Spatial frequency spectrum of the x-ray scatter distribution in CBCT projections - Bootsma - 2013 - Medical Physics - Wiley Online Library.”

<https://aapm.onlinelibrary.wiley.com/doi/full/10.1118/1.4822484> (accessed Mar. 22, 2021).

[34] F. Wang *et al.*, “Phase imaging with an untrained neural network,” *Light Sci. Appl.*, vol. 9, no. 1, Art. no. 1, May 2020, doi: 10.1038/s41377-020-0302-3.